Journal of Materials Chemistry A

Accepted Manuscript

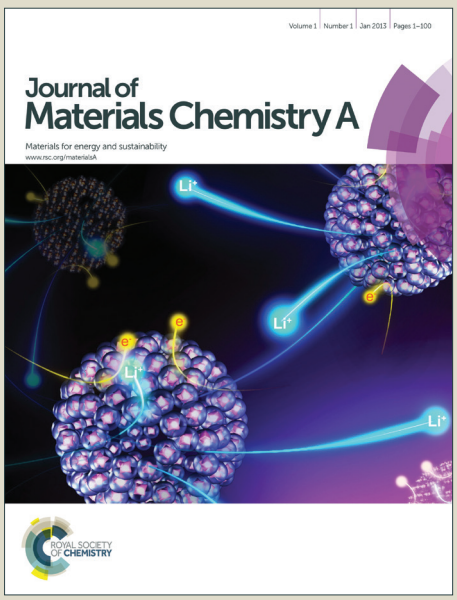

ROYAL SOCIETY OF CHEMISTRY

www.rsc.org/materialsA

J Mater Chem A

RSCPublishing

ARTICLE

Covalently-grafted Polyethyleneimine on Hydroxylated Three-dimensional Graphene for Superior CO_2 Capture

Cite this: DOI: 10.1039/x0xx00000x

Received 00th January 2015,
Accepted 00th January 2015

DOI: 10.1039/x0xx00000x

www.rsc.org/

Fa-Qian Liu,*[a] Wei Li,[a] Jie Zhao, [b,c] Wei-Hua Li,*[b,c] Dong-Mei Chen, [a] Li-Shui Sun, [a] Lei Wang,[a] and Rong-Xun Li [a]

Covalently tethered CO_2 adsorbents are synthesized by acid catalyzed ring-opening polymerization of aziridine on the basal planes of three-dimensional hydroxylated graphene (HG). The resulting materials possess high surface areas, strong covalent bonds between polyethyleneimine (PEI) and graphene, and high thermal conductivity. The HG-PEI nanocomposites exhibit high amine loading (more than 10.03 mmol N g^{-1}), high adsorption capacity (up to 4.13 mmol CO_2 g^{-1} in simulated ambient air under 1 atm of dry CO_2) as well as good stability both in low (100 ℃) and high desorption temperature (135 ℃), which allows the overall CO_2 capture process to be promising and sustainable.

Introduction

Large-scale burning of fossil fuels has caused steady increase of atmospheric CO_2 concentration, from *ca.* 315 ppm in March 1958 to more than 396 ppm today.[1] Considering the predicted detrimental effects (*e.g.*, global climate warming and anthropogenic climate change) of CO_2 emission, worldwide effort has been made to develop new materials and technologies for carbon capture and sequestration (CCS) in recent years.[2] Since their implementation in the 1930s, liquid-amine-based solution CO_2 absorption/desorption systems have been well developed and are believed to be commercially available within the next decade. However, a series of inherent problems exist, including corrosion, high energy consumption, and degradation, resulting in large operating cost. [3, 4] In this context, solid amine-based adsorbent is a promising candidate because of its excellent adsorption selectivity to CO_2, low capital cost and low energy for regeneration. [2, 5] Nevertheless, solid amine-based adsorbents suffer from problems that prohibit their widespread application. For example, the leaching problem of amines and the slow diffusion kinetics of CO_2 to active sites limit their long-term stability when amines are impregnated into the silica support. [6] In addition, covalently tethered CO_2 adsorbents prepared by post-synthesis grafting and in situ polymerization generally suffer from low CO_2 capacities. [2, 7] Most importantly, the high chemical adsorption enthalpy (ΔH) accompanied with low thermal conductivity of silica support can cause over-heating of silica support during the CO_2 capture, resulting in partial degradation of polymer amines and decomposition of silica support, finally leading to poor cycle stability. [8-10]

As an alternative solution, carbon-based materials (porous carbon, carbon nanotubes, and carbon nanofibers) have been extensively developed for CO_2 capture due to their large surface area, low cost, and fast adsorption kinetics. Nevertheless, the CO_2 adsorption on carbon materials is essentially "physisorption", which leads to high sensitivity in temperature and relatively low selectivity in operation. [11] Recently, graphene, a single-atom-thick carbon material with high specific surface area and low production cost, has been successfully applied in CO_2 capture. [12-15] Much effort has been focused on graphene-inorganic hybrid materials [12, 15, 16] and N-doped porous graphene sheets.[17] For example, a graphene-based porous silica composite material in which polyethyleneimine was physically impregnated into the mesoporous silica showed high loading content of PEI.[12] While graphene-inorganic composite adsorbents demonstrate promising performance, their synthesis is usually complicated and challenging for large-scale application, and these materials generally suffer from slow CO_2 diffusion kinetics, which is the dominant factor when the materials are operated under ambient conditions. [18]

Recently, three-dimensional (3D) graphene-based composites with interconnected pathways have attracted increasing interest, since they can exhibit minimized diffusive resistance to mass and ion transport from

macropores and a high surface area for active site dispersion from micro- and/or mesopores. [18] Herein, we report hydroxylated porous three-dimensional (3-D) graphene as a scaffold to produce a covalently-grafted graphene-polyethyleneimine (PEI) nanocomposite, exhibiting superior adsorption capacity, fast CO_2 diffusion kinetics, rapid thermal transfer, as well as good multicycle stability by a one-step reaction between aziridine and the hydroxylated graphene (HG) surface.

Experimental

Synthesis of Hydroxylated Graphene (HG). In a typical preparation process, 0.5 g pristine graphene (0.5 g) was added to the aqueous KOH (2.8g) solution (3.33 M, 15 mL). After being sonicated for 1 h, the resulting mixture was transferred into a Teflon-lined autoclave (20 mL). The sealed autoclave was heated to 180 ℃ for 6h. After the autoclave was cooled, the reaction mixture was washed with methanol and deionized (DI) water and then dried by freeze-drying, to give HG as a black solid.

Synthesis of Hydroxylated Graphene–Polyethyleneimine (HG-PEI). Aziridine was synthesized according to the previous report.[19] Typically, 255 mg (0.51:1 aziridine-to-HG ratio, w w^{-1}), 515 mg (1.03:1), 750 mg (1.50 : 1), or 990 mg (1.98 : 1) of aziridine were added to a suspension of 0.5g dried HG in toluene. Approximately 120 mg of glacial acetic acid was added to the suspension to catalyze the surface polymerization. The mixture was vigorously stirred at RT for 48 h in a sealed vessel. After completion, the powder was filtered and washed with toluene and finally dried in vacuum. The as-prepared adsorbents were denoted as HG-PEI-X, where X denotes the aziridine-to-HG ratio (w/w).

CO_2 Capture and Regeneration. CO_2 capture experiment was performed under anhydrous conditions using a TGA/DSC 2 thermogravimetric analyzer. First, about 20 mg of the as-synthesized adsorbent was pre-treated under argon at 110 ℃ for 120 min to eliminate the moisture and CO_2 adsorbed from the air. Then, the temperature was lowered to the expected temperature (25, 50 or 75 ℃) for 60 min until the weight change was lower than 0.002 mg min^{-1}. Finally, the capture curve of CO_2 could be obtained after exposing the adsorbent to a simulated flue gas (10% CO_2 balanced with argon) for 60 min. To regenerate the adsorbent, the CO_2 saturated adsorbent was switched from simulated flue gas to pure Ar (30 mL min^{-1}) and the temperature was improved to 100 ℃ (or 135 ℃) for 60 min. The CO_2 adsorption isotherms were obtained using a static volumetric analyzer (ASAP2020, Micromeritics). The high pressure CO_2 adsorption capacities (0-7 atm) of HG-PEI adsorbents were measured with a high pressure volumetric analyzer (Micromeritics HPVA-100). Typically, about 50 mg of the as-synthesized adsorbent was used. Before the experiment, the samples were pre-treated under vacuum at 110 ℃ for 12h to eliminate the moisture and CO_2 adsorbed from the air.

Characterization. The morphology of HG and HG-based adsorbents was studied on a JSM-7500F field-emission scanning electron microscope (SEM) and a JEOL 100CX transmission electron microscope (TEM). Amine content of HG-based adsorbents was measured on Flash EA1112 (Thermo Finnigan Inc. Italy). The thermogravimetric analysis was studied using a TGA/DSC 2 thermogravimetric analyzer (Mettler-Toledo AG) in nitrogen up to 900 ℃. FT-IR spectra were obtained from KBr disk on the Bruker Tensor 27 spectrometer. X-ray diffraction (XRD) patterns were recorded on a Scintag diffractometer. Solid-state ^{13}C NMR was performed on a Bruker DSX300 instrument. The Brunauer-Emmett-Teller (BET) method was used to calculate the specific surface areas of dried samples in a Micromeritics ASAP 2020 nitrogen adsorption apparatus at 77K, and the Barrett–Joyner–Halenda (BJH) model was utilized to obtain the pore size distributions from the desorption isotherms. Surface characterizations were performed with X-ray photoelectron spectroscopy (XPS, ESCALAB MK II).

Results and Discussion

The surface polymerization of aziridine on hydroxyl groups-rich substrate was first reported by Kim, [20] and then adapted to porous silica or other oxide supports by Hicks, [19] Drese, [21], Chaikittisilp,[22] and our group.[5] In the case of graphene, the hydroxyl group lied on the basal plane of the graphene has received only minor attention despite of its capability of converting to various organic functionalities, [23, 24]. Here, we report the in situ ring-opening polymerization of PEI on HG scaffold, which is illustrated in Fig.1. First, a alkaline-mediated hydrothermal treatment of graphene at 180 ℃ was employed to graft hydroxyl groups homogeneously onto the graphene nanosheets, followed by freeze-drying to give a 3-D porous structure. Next, PEI was covalently tethered onto the 3-D HG support surface by ring-opening polymerization. The as-prepared adsorbents were denoted as HG-PEI-X, where X denotes the aziridine-to-HG ratio (w/w).

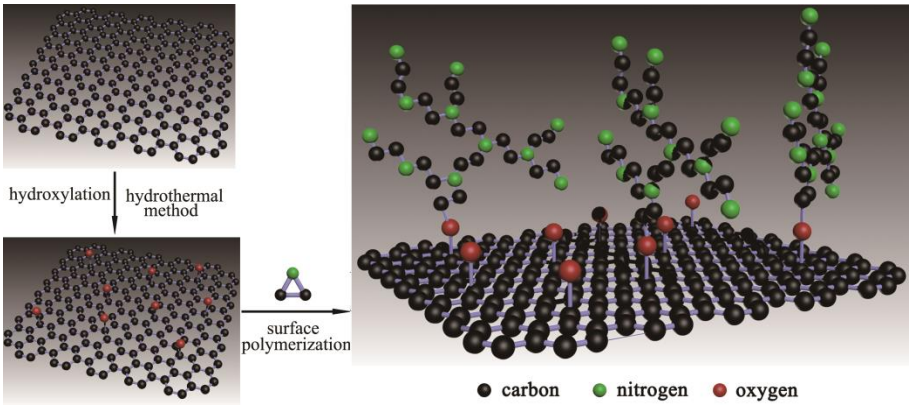

Fig. 1 Schematic illustration of the synthesis process of hydroxylated graphene–polyethyleneimine (HG-PEI) nanocomposite.

The microstructure of the as-prepared HG and the HG-PEI nanocomposites were characterized by scanning electron microscopy (SEM) and transmission electron microscope (TEM). Fig. 2a shows that honeycomb-like cellular structure consisted of slightly crinkly hydroxylated graphene sheets are formed by the sublimation of ice crystals in the freeze-drying process. [25] The size of the 3-D HG macroporous scaffold is on the order of several to several tens of micrometers. Fig. S1 shows the TEM image of HG. The elemental oxygen mapping (Fig. S2) shows the uniform distriction of hydroxyl groups on the surface of HG. The hyperbranched PEI was synthesized on 3-D HG via a one-step in situ surface polymerization between aziridine and hydroxyl group as previously reported,[19, 26] giving rise to a chemically grown PEI thin film uniformly covered on the 3-D HG scaffold (Fig. S3). The successful in situ polymerization of PEI was further verified by the rough surface of HG after the polymerization of PEI (Fig. 2b). The elemental mapping, shown in Fig. 2c and Fig. 2d, presents homogenous distribution of carbon and nitrogen in the HG-PEI nanocomposite, further indicating that PEI is densely grown and highly-dispersed on anchoring hydroxyl groups of the HG scaffold.

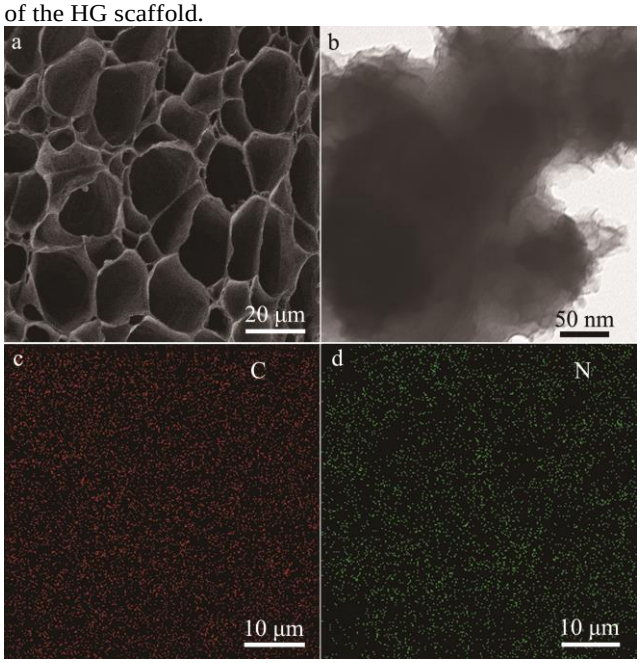

Fig. 2 SEM and EDS mapping image of HG and HG-PEI nanocomposites: (a) SEM image of the 3-D graphene, (b) TEM image of HG-PEI-1.98, (c) EDS carbon mapping for the region shown in (b), and (d) EDS nitrogen mapping for the region shown in (b).

The surface characteristics of the HG-PEI nanocomposite were studied by the X-ray photoelectron spectroscopy (XPS) and Fourier transform infrared (FTIR) spectra. The full survey XPS analysis (Fig. S4) at 399.8 eV and 533.1 eV clearly indicates that N and O elements exist in the HG-PEI nanocomposite.[12] High-resolution XPS C1s spectrum of HG demonstrates three overlapped peaks at 284.6, 285.4, and 286.1 eV, which are attributed to the sp^2 carbon (C = C), sp^3 carbon(C-C), and hydroxylated carbon (C-OH), respectively (Fig. 3a).[27,28] Contrary to HG, The intensity of C1s spectrum of HG-PEI nanocomposite decreases due to the coverage of PEI on the graphene surface(Fig. 3b). Specifically, the peak intensity of the hydroxylated carbon reduces significantly, showing possible partial cleavage of the C-OH bond during the surface polymerization. FTIR spectra of hydroxylated graphene and covalently-grafted HG-PEI are shown in Fig. 3c. The strong broad band centered at 3437 cm^{-1} and weak band at 1320 $cm^{-1}$are assigned to the stretching and bending vibration of OH groups in an enol C=C–OH form on the basal planes, respectively. [29, 30] The absorption peak appears at ~1600 cm^{-1} is ascribed to the skeletal vibration of the graphene.[31] After the surface polymerization reaction, the existence of PEI is evidenced by the presence of absorption feature of PEI at 3288, 2940, and 2827 cm^{-1}. [32] The XRD patterns of HG before and after the polymerization of PEI were shown in Fig. S5. The similar peak positions indicate that the 3-D structure of the HG scaffold was preserved after the surface polymerization of PEI. [29] However, the diffraction intensity of the HG-based amine adsorbents decreases as the amine loading increases, indicating that the pores are filled by PEI.

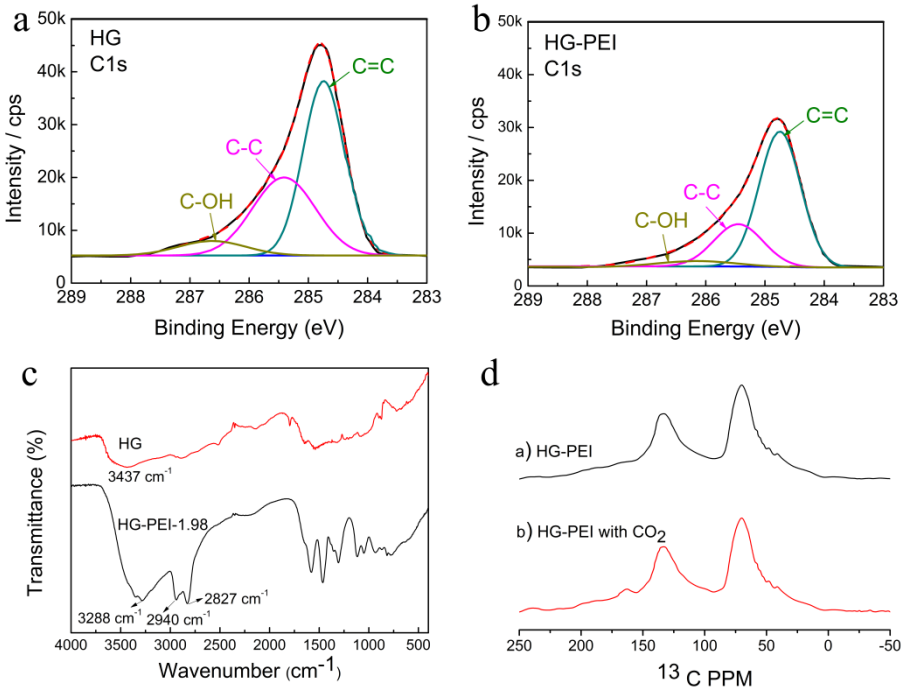

Fig. 3 High-resolution C1s XPS spectra and the corresponding Gaussian fitting results (three peaks for different bonded carbon) of (a) HG and (b) HG-PEI-1.98, the sum of fitting spectra (red dashed line) is in agreement with the raw spectra (black solid line). (c) FT-IR spectra of HG and HG-PEI-1.98. (d) Solid state ^{13}C MAS NMR of HG-PEI with or without CO_2.

The Brunauer–Emmett–Teller (BET) nitrogen adsorption/desorption measurements give surface areas of 193.51, 119.17, 76.50, 38.93, and 17.05 m^2/g for HG, HG-PEI-0.51, HG-PEI-1.03, HG-PEI-1.50, and HG-PEI-1.98, respectively (Fig. S6). The characteristics of fundamental type II isotherm together with type H3 hysteresis loop around 1.0 P/P_0 were observed for HG and all the HG-based adsorbents, which indicate the abundance of macropores in the HG-based adsorbents. [33-36] We also noticed the relatively less reduction of volume of nitrogen adsorbed after grafting with amine, which may be due, in part, to the 3-D macroporous structure.[5, 37] The corresponding pore size distribution is shown in Fig. S7, indicating that the pore sizes are in the range of 1-100 nm. The big pores with sizes larger than 100 nm, which are observed by the SEM, can't be detected by the N_2 adsorption measurements.[5] Fig. S8 shows that hydroxylated graphene is stable under nitrogen when temperature is lower than 400 ℃, while both commercial PEIs with molecular weights of 10000 and 600 decompose completely at ~400 ℃. So, The PEI contents of HG-PEI-0.51, HG-PEI-1.03, HG-PEI-1.50, and HG-PEI-1.98 were estimated to be ~18, 28, 37 and 42 wt %, respectively, based on the combined TGA weight loss under nitrogen.

The CO_2 capture behavior of HG-based adsorbents was evaluated by TGA in simulated flue gas (10% CO_2 balanced with argon) at the conditions of 25-75 ℃. Pellets with sizes from 1 to 2 mm were collected and conducted for tests. As shown in Fig. S9, the PEI layer is composed of nanoparticles with sizes from several to several tens of nanometers. Solid ^{13}C CP MAS NMR spectra for the HG-based adsorbent before and after exposure to CO_2 are shown in Fig. 3d. The resonance centered at 134 ppm is assigned to unoxidized sp^2 carbons, and the 70 ppm resonance corresponds to hydroxylated carbons. [38] The weak shoulder peaks from 40 to 60 ppm are assigned to the different carbon atom environments in the polyethylenimine.[22] After contact with CO_2, the peak at 164.2 ppm is assigned to the carbamate ions formed by reaction of amine with CO_2. [5, 39] The CO_2 capture capacities and amine efficiencies at different temperatures are summarized in Table 1. The HG-PEI-1.98 sample displays a maximum adsorption capacity of 4.13 mmol g^{-1} at 25 ℃ and 1 atm (Fig. 4a), which is among the best behaved low-temperature solid amine-based CO_2 adsorbents. *i.e.*,4.23 mmol g^{-1} for nano silica impregnated with PEI, [40] 3.86 mmol g^{-1} for amine-tethered adsorbents based on three-dimensional macroporous silica.[5] The adsorption capacity is also comparable to other low-temperature solid adsorbents. A graphical illustration of selected low-temperature solid CO_2 adsorbents performance since 2008 with appropriate references is shown in Fig. 5. CO_2 adsorption capacity at high pressure was further evaluated (Fig. S10). The highest volumetric CO_2 uptake was recorded for HG-PEI-1.98 which exhibits 4.63 mmol g^{-1} uptake at 25 ^oC / 7 atm.

The chemically tethered nature was demonstrated in Fig. 4b. It has long been taken for granted that the temperature dependency is almost always the case when mesoporous

supports are used and the amines are physically adsorbed (impregnation). The maximum CO_2 adsorption capacity over these adsorbents occurs around 75-90 ℃ as a result of the diminished diffusion resistance, resulting in a nonintuitive functional dependence of the CO_2 adsorption with the temperature (inverse Van't Hoff behavior). [41, 42] However, as demonstrated in Fig. 4b, we show a different temperature dependency of the maximal CO_2 adsorption when the amines are chemically tethered to the support. With the increase of the adsorption temperature from 25 to 75 ℃, the CO_2 adsorption capacity of HG-PEI adsorbents decreases substantially as a result of exothermic adsorption reaction (Van't Hoff behavior), favored at low adsorption temperature. This observation is probably associated with the fast mass transfer in these HG-PEI adsorbents. The 3-D interconnected macroporous structure along with the uniform distribution of PEI on the HG surfaces provides low resistant pathways for the diffusion of CO_2 molecules. As a result, the adsorption of CO_2 over HG-based adsorbents was strongly dominated by the thermodynamic factor rather than kinetic diffusion. Similar results have been observed for covalently attached silica adsorbents reported before. [19, 21, 22] The adsorption enthalpies, calculated from the DSC heatflow profiles during adsorption process (Fig. S11), are in the range 62-68 kJ/mol (Table 1), which correspond to the values of chemical adsorption, indicating that the adsorption interactions between CO_2 and the HG-PEI adsorbents are strong enough to guarantee the excellent adsorption selectivity of CO_2 over water.[43]

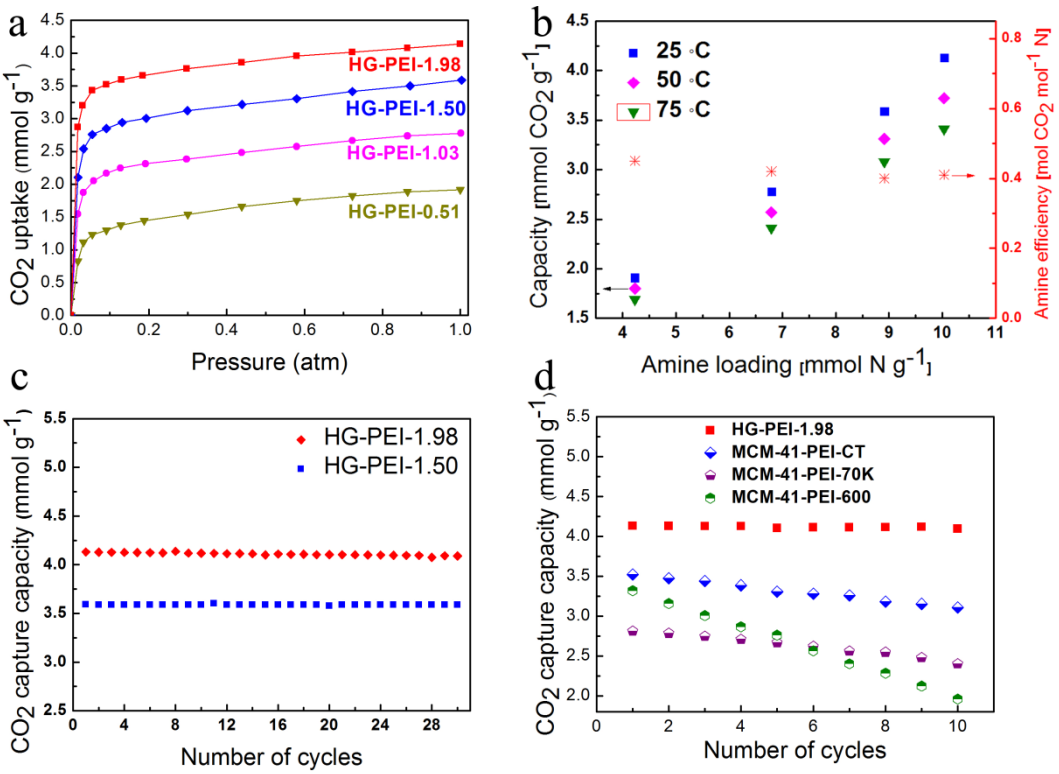

Fig. 4 (a) CO_2 adsorption isotherms measured at 298 K. (b) CO_2 capture capacities in 10% CO_2 at 25, 50, and 75 ℃ and associated amine efficiency at 25 ℃ versus amine loadings of the HG-PEI adsorbents. (c) The CO_2 adsorption/desorption cyclic stability of HG-PEI-1.98 and HG-PEI-1.50. Experimental conditions: adsorption at 25 ℃ for 60 min in 10% CO_2 and desorption at 100 ℃ for 60 min in 100% argon. (d) The CO_2 adsorption/desorption cyclic stability of HG-PEI-1.98 and MCM-41-PEI-based adsorbents. Experimental conditions: adsorption at 25 ℃ for 60 min in 10% CO_2 and desorption at 135 ℃ for 60 min in 100% argon.

Table 1. CO_2 adsorption characteristics of HG-PEI adsorbents under dry conditions

Sample	Amine loading [mmol N g^{-1}]	Capacity [mmol CO_2 g^{-1}]			Amine efficiency [mol CO_2 N^{-1}]			Adsorption enthalpies (kJ/mol) [a]
		25 ℃	50 ℃	75 ℃	25 ℃	50 ℃	75 ℃	
HG-PEI-0.51	4.23	1.91	1.80	1.69	0.45	0.43	0.40	62
HG-PEI-1.03	6.79	2.78	2.57	2.41	0.41	0.38	0.35	65
HG-PEI-1.50	8.91	3.59	3.31	3.08	0.40	0.37	0.35	66
HG-PEI-1.98	10.03	4.13	3.72	3.41	0.41	0.37	0.34	68

[a] adsorption at 25 ℃

These HG-based adsorbents also exhibit excellent capture kinetics. As shown in Fig. S12a, the conversion of all the four HG-PEI adsorbents reaches half of their final capacity within a short gas-solid contact time of ~1-2 min, and 80% of their final capacity within ~10 min. The adsorption kinetics are comparable to those of amine-functionalized mesoporous adsorbents reported before, *i.e.* 80 % of the equilibrium CO_2 capacity was reached in 30 minute for 3-aminopropyl-functionalized MCM-48 sample under dry conditions.[44] We also noticed that the CO_2 adsorption into PEI occurs in two stages. The fast gas-solid surface chemical reaction between CO_2 and amines governs the first stage, followed by a relatively slow uptake controlled by the diffusion of CO_2 into the lower PEI multilayers. Fig. S12b shows that the adsorption halftimes also increase with the amine loading because of the limited accessibility of CO_2 to the amine sites. [5, 22, 45, 46]

Based on the high adsorption capacity of 4.13 mmol g^{-1} in simulated flue gas and the chemical nature of the CO_2-amine interactions (Table 1), heat-driven regeneration mode was selected to evaluate the stability of postcombustion CO_2 capture using simulated flue gas (10% CO_2).[5, 47, 48] Fig. 4c shows the adsorption-desorption cycles of HG-PEI-1.98 and HG-PEI-1.50. The CO_2 adsorption/desorption profile of HG-PEI-1.98 is shown in Fig. S13. The CO_2 capture capacity decreases only ~1% after 30 cycles for both adsorbents, which can be assigned to the high boiling point of PEI, high thermal conductivity of graphene, and strong chemical bonds of carbamate ion pairs between PEI and CO_2. As a conventional mesoporous molecular sieve, MCM-41 has large pore volume, high adsorption capacity and synergetic effect on the adsorption of CO_2 by PEI. [49] So, to further verify the effects of graphene as an excellent thermal conductor, conventional MCM-41 impregnated with PEI of different molecular weights (denoted as MCM-41-PEI-X, where X denotes the molecular weight) and chemically tethered PEI adsorbents based on the MCM-41 (denoted as MCM-41-PEI-CT) were also prepared and evaluated under the same conditions. The powder X-ray diffraction pattern of MCM-41 is shown in Fig. S14. N_2-sorption isotherm and pore size distribution of all PEI-MCM-41-based adsorbents are shown in Fig. S15 and Fig. S16, respectively. The fast capacity loss was observed for all the three MCM-41-based adsorbents when desorption temperature was improved from 100 to 135 ℃ (Fig. 4d). In contrast, the capture capacity of HG-PEI-1.98 was very stable during the regeneration process. Given that the CO_2-adsorbent interactions for both MCM-41-PEI-CT and HG-PEI-1.98 are chemical in nature, the stable cycling of HG-based adsorbents is indubitably attributed to the high thermal conductivity of graphene. As a result, the 3-D hydroxylated graphene scaffold can efficiently transfer the heat out of the adsorbent matrix and finally prevent the degradation of PEI.

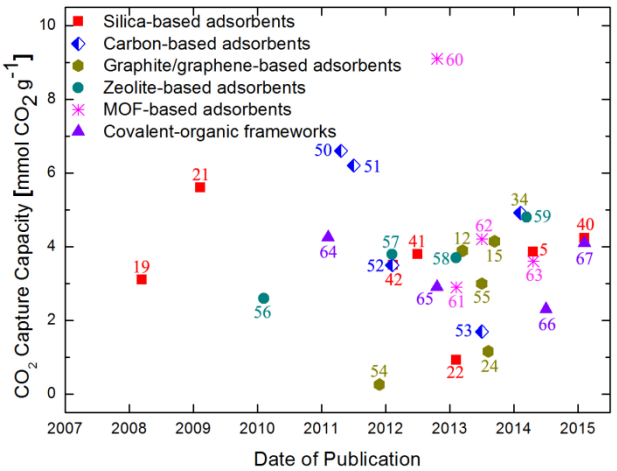

Fig. 5 Selected low-temperature solid CO_2 adsorbents performance progress since 2008. Red squares = silica-based adsorbents, [5, 19, 21, 22, 40-42] blue diamonds = carbon-based adsorbents, [34, 50-53] dark yellow hexagons = graphite/graphene-based adsorbents, [12, 15, 24, 54, 55] dark cyan circles = zeolite-based adsorbents, [56-59] magenta stars = MOF-based adsorbents, [60-63] and violet uptriangles = covalent-organic frameworks. [64-67] Each point is labeled with the corresponding reference number.

Conclusions

In conclusion, a new type of HG-PEI nanocomposite, in which polyethyleneimine was uniformly covalently-grafted to the graphene basal surfaces, has been developed through acid catalyzed surface polymerization at room temperature. The HG-PEI nanocomposites exhibit high adsorption capacity as well as good stability both in low and high desorption temperature. This improvement could be attributed to (i) the 3-D macroporous morphology, which minimizes not only the diffusive resistance of CO_2 to the active adsorption sites, but also the susceptibility of pore blockage as the amine content increases, (ii) the uniformly distributed strong covalent bonds between PEI and hydroxylated graphene, which guarantees the high adsorption efficiency and good cyclic stability, (iii) the high thermal conductivity of graphene that allows fast transfer of heat and avoids the degradation of the organic amines. We believe that the 3-D HG-PEI nanocomposite with excellent thermal conductivity is a promising material for practical carbon capture and sequestration.

Acknowledgements

FL acknowledges the support from the National Science Foundation of China (21371105 and 51372125) and the Scientific Development Plan of Qingdao (14-2-4-41-jch). WL acknowledges the support from the National Science Foundation of China (51179182) and the Distinguished Young Scientists Funds of Shandong (2012JQF01002). LS acknowledges the support from the National Science Foundation of China (51402162).

Notes and references

[a] Engineering Research Center of High Performance Polymer and Molding Technology, Ministry of Education, Qingdao University of Science and Technology, Qingdao 266042, China. E-mail: faqianliu@yahoo.com
[b] Cooperative Innovation Center of Engineering Construction and Safety in Shandong Blue Economic Zone, Qingdao Technological University, Qingdao 266033, China. E-mail: 1685680@163.com
[c] Institute of Oceanology, Chinese Academy of Sciences, Qingdao 266071, China.

† Electronic Supplementary Information (ESI) available: [SEM and TEM images, full survey XPS spectrum, XRD patterns, nitrogen adsorption/desorption isotherms, pore size distribution, TGA thermograms, DSC heatflow profiles, CO_2 capture kinetics and adsorption halftimes, CO_2 adsorption/desorption profile,]. See DOI: 10.1039/b000000x/

1. E. Kintisch, *Science*, 2008, **320**, 306-308.
2. J. Wang, L. Huang, R. Yang, Z. Zhang, J. Wu, Y. Gao, Q. Wang, D. O'Hare and Z. Zhong, *Energy Environ. Sci.*, 2014, **7**, 3478-3518.
3. E. B. Rinker, S. S. Ashour and O. C. Sandall, *Ind. Eng. Chem. Res.*, 2000, **39**, 4346-4356.
4. R. S. Franchi, P. J. E. Harlick and A. Sayari, *Ind. Eng. Chem. Res.*, 2005, **44**, 8007-8013.
5. F.-Q. Liu, L. Wang, Z.-G. Huang, C.-Q. Li, W. Li, R.-X. Li and W.-H. Li, *ACS Appl. Mater. Interfaces*, 2014, **6**, 4371-4381.
6. A. Goeppert, S. Meth, G. K. S. Prakash and G. A. Olah, *Energy Environ. Sci.*, 2010, **3**, 1949-1960.
7. P. Bollini, S. A. Didas and C. W. Jones, *J. Mater. Chem.*, 2011, **21**, 15100-15120.
8. W. Li, P. Bollini, S. A. Didas, S. Choi, J. H. Drese and C. W. Jones, *ACS Appl. Mater. Interfaces*, 2010, **2**, 3363-3372.
9. V. Krungleviciute, A. D. Migone, M. Yudasaka and S. Iijima, *J. Phys. Chem. C*, 2011, **116**, 306-310.
10. R. Roque-Malherbe, R. Polanco-Estrella and F. Marquez-Linares, *J. Phys. Chem. C*, 2010, **114**, 17773-17787.
11. T. C. Drage, O. Kozynchenko, C. Pevida, M. G. Plaza, F. Rubiera, J. J. Pis, C. E. Snape and S. Tennison, *Energy Procedia*, 2009, **1**, 599-605.
12. S. Yang, L. Zhan, X. Xu, Y. Wang, L. Ling and X. Feng, *Adv. Mater.*, 2013, **25**, 2130-2134.
13. L.-Y. Meng and S.-J. Park, *J. Colloid Interface Sci.*, 2012, **386**, 285-290.
14. A. K. Mishra and S. Ramaprabhu, *J. Mater. Chem.*, 2012, **22**, 3708-3712.
15. A. A. Alhwaige, T. Agag, H. Ishida and S. Qutubuddin, *RSC Adv.*, 2013, **3**, 16011-16020.
16. Y. Zhu, S. Murali, W. Cai, X. Li, J. W. Suk, J. R. Potts and R. S. Ruoff, *Adv. Mater.*, 2010, **22**, 3906-3924.
17. V. Chandra, S. U. Yu, S. H. Kim, Y. S. Yoon, D. Y. Kim, A. H. Kwon, M. Meyyappan and K. S. Kim, *Chem. Commun.*, 2012, **48**, 735-737.
18. S. Dutta, A. Bhaumik and K. C. W. Wu, *Energy Environ. Sci.*, 2014, **7**, 3574-3592.
19. J. C. Hicks, J. H. Drese, D. J. Fauth, M. L. Gray, G. G. Qi and C. W. Jones, *J. Am. Chem. Soc.*, 2008, **130**, 2902-2903.
20. H. J. Kim, J. H. Moon and J. W. Park, *J. Colloid Interface Sci.*, 2000, **227**, 247-249.
21. J. H. Drese, S. Choi, R. P. Lively, W. J. Koros, D. J. Fauth, M. L. Gray and C. W. Jones, *Adv. Funct. Mater.*, 2009, **19**, 3821-3832.
22. W. Chaikittisilp, S. A. Didas, H. J. Kim and C. W. Jones, *Chem. Mater.*, 2013, **25**, 613-622.
23. M. Melucci, E. Treossi, L. Ortolani, G. Giambastiani, V. Morandi, P. Klar, C. Casiraghi, P. Samori and V. Palermo, *J. Mater. Chem.*, 2010, **20**, 9052-9060.
24. S.-M. Hong, S. H. Kim and K. B. Lee, *Energy Fuels*, 2013, **27**, 3358-3363.
25. L. Qiu, J. Z. Liu, S. L. Y. Chang, Y. Wu and D. Li, *Nat Commun*, 2012, **3**, 1241.
26. W. R. Collins, W. Lewandowski, E. Schmois, J. Walish and T. M. Swager, *Angew. Chem. Int. Ed.*, 2011, **50**, 8848-8852.
27. P. Gong, J. Wang, W. Sun, D. Wu, Z. Wang, Z. Fan, H. Wang, X. Han and S. Yang, *Nanoscale*, 2014, **6**, 3316-3324.
28. F. Gao, D. Zeng, Q. Huang, S. Tian and C. Xie, *Phys. Chem. Chem. Phys.*, 2012, **14**, 10572-10578.
29. C. Zu and A. Manthiram, *Adv. Energy Mater.*, 2013, **3**, 1008-1012.
30. D. Yang, G. Guo, J. Hu, C. Wang and D. Jiang, *J. Mater. Chem.*, 2008, **18**, 350-354.
31. H. Zhang, X. Lv, Y. Li, Y. Wang and J. Li, *ACS Nano*, 2009, **4**, 380-386.
32. C. Shan, L. Wang, D. Han, F. Li, Q. Zhang, X. Zhang and L. Niu, *Thin Solid Films*, 2013, **534**, 572-576.
33. F.-Q. Liu, H. Wu, T. Li, L. R. Grabstanowicz, K. Amine and T. Xu, *Nanoscale*, 2013, **5**, 6422-6429.
34. J. Wang and Q. Liu, *Nanoscale*, 2014, **6**, 4148-4156.
35. F.-Q. Liu, J. Su, W. Wang, W.-H. Li, H.-Q. Hu, L. Wang and R.-X. Li, *J. Mater. Chem. A*, 2015, **3**, 3136-3143.
36. F.-Q. Liu, W.-H. Li, B.-C. Liu and R.-X. Li, *J. Mater. Chem. A*, 2013, **1**, 8037-8044.
37. B. G. Choi, M. Yang, W. H. Hong, J. W. Choi and Y. S. Huh, *ACS Nano*, 2012, **6**, 4020-4028.
38. Y. Si and E. T. Samulski, *Nano Lett.*, 2008, **8**, 1679-1682.
39. E. P. Dillon, C. A. Crouse and A. R. Barron, *ACS Nano*, 2008, **2**, 156-164.
40. K. Li, J. Jiang, S. Tian, F. Yan and X. Chen, *J. Mater. Chem. A*, 2015, **3**, 2166-2175.
41. T. Witoon, *Mater. Chem. Phys.*, 2012, **137**, 235-245.
42. T. Witoon and M. Chareonpanich, *Mater. Lett.*, 2012, **81**, 181-184.
43. S. Choi, J. H. Drese, P. M. Eisenberger and C. W. Jones, *Environ. Sci. Technol.*, 2011, **45**, 2420-2427.
44. H. Y. Huang, R. T. Yang, D. Chinn and C. L. Munson, *Ind. Eng. Chem. Res.*, 2002, **42**, 2427-2433.
45. J. D. Lunn and D. F. Shantz, *Chem. Mater.*, 2009, **21**, 3638-3648.
46. W. Chaikittisilp, J. D. Lunn, D. F. Shantz and C. W. Jones, *Chem. Eur. J.*, 2011, **17**, 10556-10561.
47. A. H. Berger and A. S. Bhown, *Energy Procedia*, 2011, **4**, 562-567.
48. G. D. Pirngruber, F. Guillou, A. Gomez and M. Clausse, *Int. J. Greenhouse Gas Control*, 2013, **14**, 74-83.
49. X. Xu, C. Song, J. M. Andresen, B. G. Miller and A. W. Scaroni, *Energy Fuels*, 2002, **16**, 1463-1469.
50. M. Sevilla and A. B. Fuertes, *Energy Environ. Sci.*, 2011, **4**, 1765-1771.
51. M. Sevilla, P. Valle-Vigón and A. B. Fuertes, *Adv. Funct. Mater.*, 2011, **21**, 2781-2787.
52. D. Wang, X. Ma, C. Sentorun-Shalaby and C. Song, *Ind. Eng. Chem. Res.*, 2012, **51**, 3048-3057.
53. M. M. Gui, Y. X. Yap, S.-P. Chai and A. R. Mohamed, *Int. J. Greenhouse Gas Control*, 2013, **14**, 65-73.
54. M. Asai, T. Ohba, T. Iwanaga, H. Kanoh, M. Endo, J. Campos-Delgado, M. Terrones, K. Nakai and K. Kaneko, *J. Am. Chem. Soc.*, 2011, **133**, 14880-14883.
55. S. Muhammad, C. Vimlesh, K. C. Kemp and S. K. Kwang, *Nanotechnology*, 2013, **24**, 255702.
56. F. Su, C. Lu, S.-C. Kuo and W. Zeng, *Energy Fuels*, 2010, **24**, 1441-1448.
57. M. R. Hudson, W. L. Queen, J. A. Mason, D. W. Fickel, R. F. Lobo and C. M. Brown, *J. Am. Chem. Soc.*, 2012, **134**, 1970-1973.
58. T.-H. Bae, M. R. Hudson, J. A. Mason, W. L. Queen, J. J. Dutton, K. Sumida, K. J. Micklash, S. S. Kaye, C. M. Brown and J. R. Long, *Energy Environ. Sci.*, 2013, **6**, 128-138.
59. C. Chen, D.-W. Park and W.-S. Ahn, *Appl. Surf. Sci.*, 2014, **292**, 63-67.
60. J. Park, J.-R. Li, Y.-P. Chen, J. Yu, A. A. Yakovenko, Z. U. Wang, L.-B. Sun, P. B. Balbuena and H.-C. Zhou, *Chem. Commun.*, 2012, **48**, 9995-9997.
61. Q. Yan, Y. Lin, P. Wu, L. Zhao, L. Cao, L. Peng, C. Kong and L. Chen, *ChemPlusChem*, 2013, **78**, 86-91.
62. Y. Lin, Q. Yan, C. Kong and L. Chen, *Sci. Rep.*, 2013, **3**, 1859.
63. Y. Hu, W. M. Verdegaal, S.-H. Yu and H.-L. Jiang, *Chemsuschem*, 2014, **7**, 734-737.
64. W. Lu, D. Yuan, J. Sculley, D. Zhao, R. Krishna and H.-C. Zhou, *J. Am. Chem. Soc.*, 2011, **133**, 18126-18129.
65. H.-L. Jiang, D. Feng, T.-F. Liu, J.-R. Li and H.-C. Zhou, *J. Am. Chem. Soc.*, 2012, **134**, 14690-14693.

66. M. Tong, Q. Yang, Y. Xiao and C. Zhong, *Phys. Chem. Chem. Phys.*, 2014, **16**, 15189-15198.
67. N. Huang, X. Chen, R. Krishna and D. Jiang, *Angew. Chem. Int. Ed.*, 2015, **54**, 2986-2990.

Table of contents

Covalently-grafted polyethyleneimine-hydroxylated three-dimensional graphene nanocomposites prepared by ring-opening polymerization exhibits superior CO_2 capture behavior.